Aquaculture 543 (2021) 736973

Contents lists available at ScienceDirect

Aquaculture

journal homepage: www.elsevier.com/locate/aquaculture

Numerical simulation of oxygen transport in land-based aquaculture tank

Guang Yin [a], Muk Chen Ong [a], Jihoon Lee [b], Taeho Kim [b,*]

[a] Department of Mechanical and Structural Engineering and Materials Science, University of Stavanger, Stavanger 4036, Norway
[b] Department of Marine Production Management, Chonnam National University, Yeosu 59626, Republic of Korea

ARTICLE INFO

Keywords:
Oxygen transport
Aquaculture tank
Computational fluid dynamics
Dissolved oxygen concentrations

ABSTRACT

Dissolved oxygen is an important indicator of the water quality and important for fish survival in aquaculture. The distribution of the dissolved oxygen is highly dependent on the flow motions, the pressure and the temperature of the water. With the development of computational fluid dynamics, the spatial and temporal distribution of dissolved oxygen in water can be predicted to evaluate and maintain the water quality. In the present study, a three-dimensional numerical model for predicting the dissolved oxygen and the water flow motions is developed. Oxygen transport in land-based aquaculture tanks is investigated by solving the Unsteady Reynolds-Averaged Navier–Stokes (URANS) equations combined with an additional species transport equation of the dissolved oxygen concentration. The volume of fluid (VOF) method is used to simulate the evolution of two-phase immiscible flows of the water and the air with an interface. The predicted dissolved oxygen concentrations (DOC) are in agreement with the experimental measurement which validate the present numerical model. The evolution of the DOC in the water and the water velocities are discussed based on the numerical simulations.

1. Introduction

Land-based fish farming are becoming a worldwide attractive method for aquaculture engineering within these years. According to Böttger et al. (2006), compared with the traditional fish farming in open water, land-based fish farming may cause less environmental impact to coastal areas and reduce the cost of transportation. By using various operations installed with the land-based aquaculture tanks, it is also easier to control diseases and parasites, and monitor the water quality based on the dissolved oxygen concentration, temperature, nutrient and suspended solids content. For example, the water can be cleaned and saturated with oxygen before being pumped into the tanks to provide a healthy living environment for fish. Compared with the open-water fish farming, by using the land-based aquaculture tanks, pollutions can be reduced, and quick adjustments can be also made to achieve optimal living conditions.

In aquaculture engineering, the dissolved oxygen concentration (DOC) can be used as a critical indicator of the water quality to maintain the survival of fish. It is of great significance to measure and control the oxygen concentration in the water to keep a healthy ecological system and achieve a good living condition for fish. Water, air and oxygen mixture flow is commonly seen in aquaculture tanks. As water and oxygen mixture continue happening through the water inlets, the dissolved oxygen concentration (DOC) changes with the water velocity and pressure in the whole aquaculture tank. In experiments, oxygen sensors are commonly placed in the water and used to monitor DOC in the aquaculture tanks. However, DOC data at only a few detection points in the aquaculture tanks can be detected by using measurement instruments. It is difficult to predict the three-dimensional spatial and temporal DOC distribution, the dissolved oxygen diffusion rate in the water and water flow velocities in the whole flow field. Analytical solutions or experiments for these hydrodynamic problems are not feasible.

Nowadays, with the rapid development of computational fluid dynamics (CFD), numerical simulations are becoming an attractive alternation to experiments for engineering design for aquaculture tanks. There are extensively studies on DOC transport in water by using numerical simulations. Kim et al. (2015) used CFD based on Reynolds Averaged Navier-Stokes equations (RANS) to investigate the flow behaviors and the distributions of DOC within a co-culture cage system. An experimentally validated numerical simulation model were developed by Fayolle et al. (2007) to predict flow and oxygen transfer characteristics in aeration tanks equipped with fine bubble diffusers and axial slow speed mixers. Dissolved oxygen (DO) transport model is developed coupled with the air-water two-phase mixture flow model and used to simulate the physical processes and predict the supersaturated DOC in

* Corresponding author.
E-mail address: kimth@chonnam.ac.kr (T. Kim).

https://doi.org/10.1016/j.aquaculture.2021.736973
Received 4 November 2020; Received in revised form 5 May 2021; Accepted 25 May 2021
Available online 27 May 2021

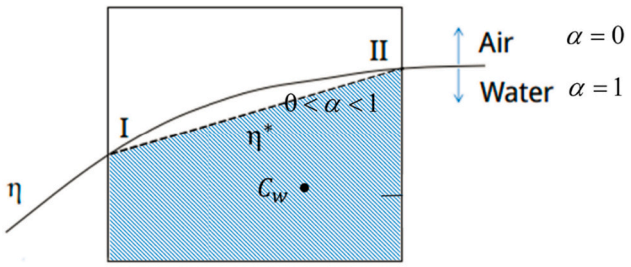

Fig. 1. A sketch of intersection between free surface of water taken from Liu et al. (2017).

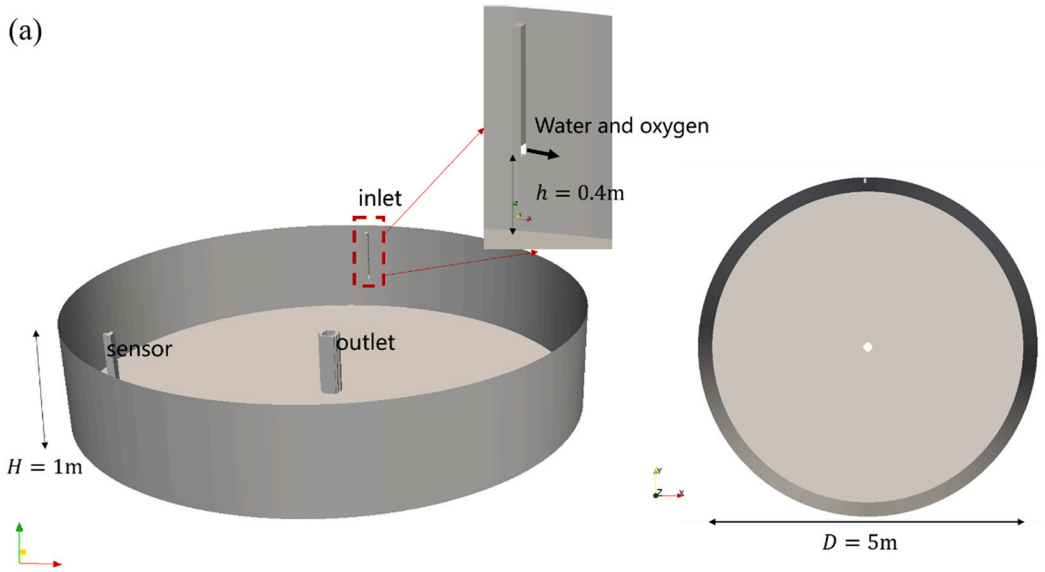

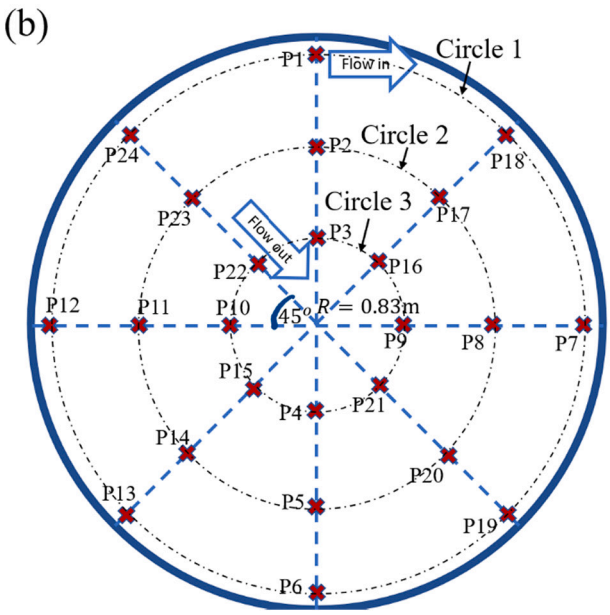

Fig. 2. (a) Geometry of the circular aquaculture tank with zoom-in views of the inlet and the top views.; (b) Locations of these 24 detection points at one 2D XY plane.

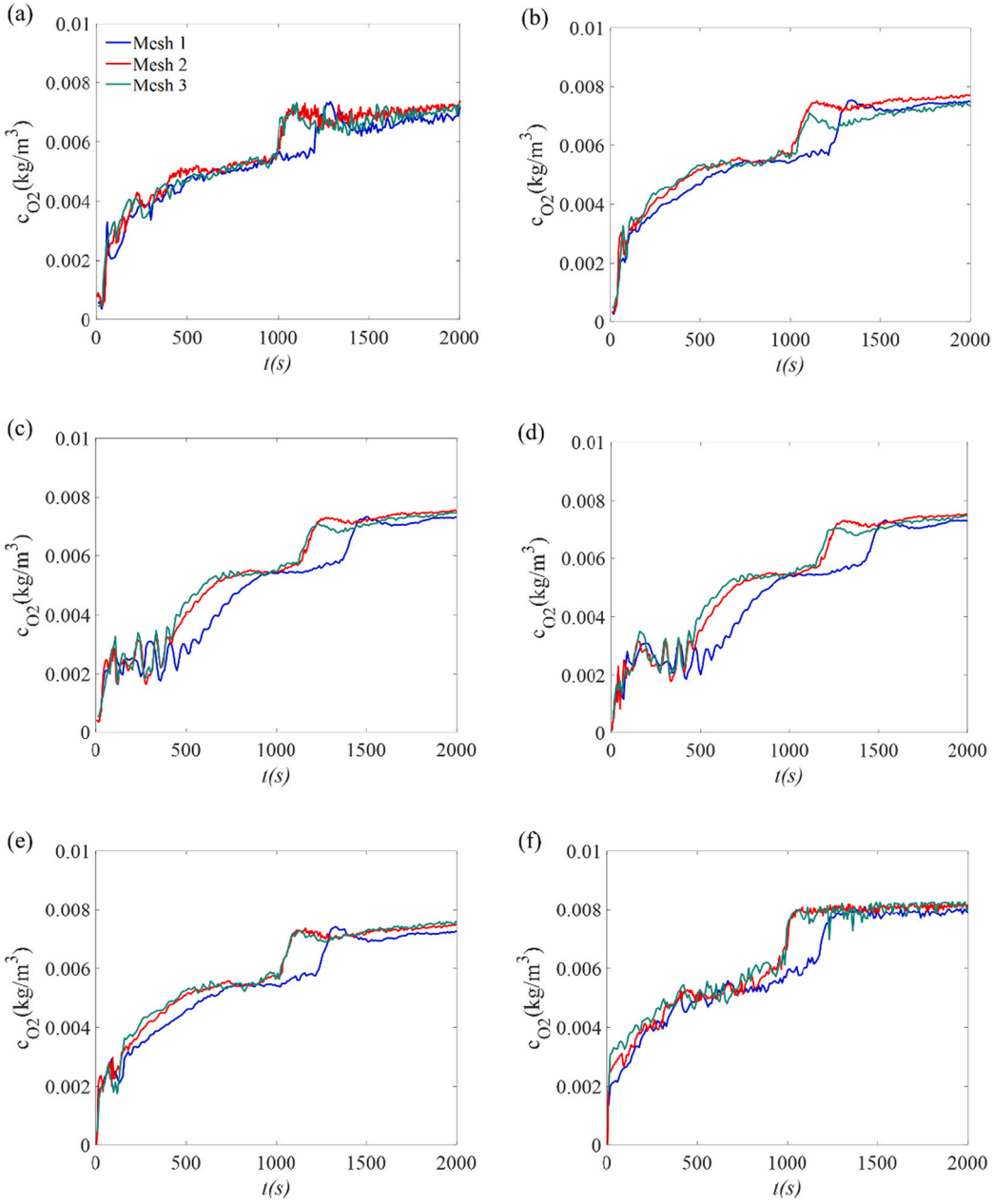

Fig. 3. The time histories of DOC at the measurement points of (a) Point 1; (b) Point 2; (c) Point 3; (d) Point 4; (e) Point 5; (f) Point 6 using different grid numbers.

the water-body downstream of a spillway by Cheng et al. (2009). An environmental CFD code was developed and used by Xia et al. (2011) to investigate the distribution of the DO as well as salinity, temperature and nutrients in open water environment such as Perdido Bay and adjacent Gulf of Mexico. A DO convection and diffusion model was established to simulate the DOC in a circular pipe, Stokes waves and horizontal venturi flow with two holes by Yin et al. (2011, 2012 and 2018). The flow velocity and DO concentration in the outer channel of an orbal oxidation ditch system in a wastewater treatment plant were simulated and monitored under actual operation conditions by Guo et al. (2013). Matko et al. (2020) used numerical simulations to predict the gas-liquid flow pattern and dissolved oxygen distribution in a wastewater treatment oxidation ditch with various aerators. The effects of the biochemical oxygen demand distribution and the bubble size distribution on the distribution of the dissolved oxygen were discussed.

In the present study, three-dimensional (3D) numerical simulations are conducted to study the multiphase flow in an aquaculture tank based on OpenFOAM, an open source computational fluid dynamics (CFD) code. The air-water interface is tracked by the volume of fluid (VOF) method. An additional convection-diffusion equation for the oxygen is solved to obtain the oxygen distribution in the whole aquaculture tank. The organization of this study is as follows: Section 2 introduce the mathematical model for the simulations. Section 3 presents the results and discussion of the numerical simulations and Section 4 gives the conclusion.

2. Mathematical model

2.1. Flow model

In the framework of CFD by using OpenFOAM, the finite volume method is used to solve the governing equations of the flow and the

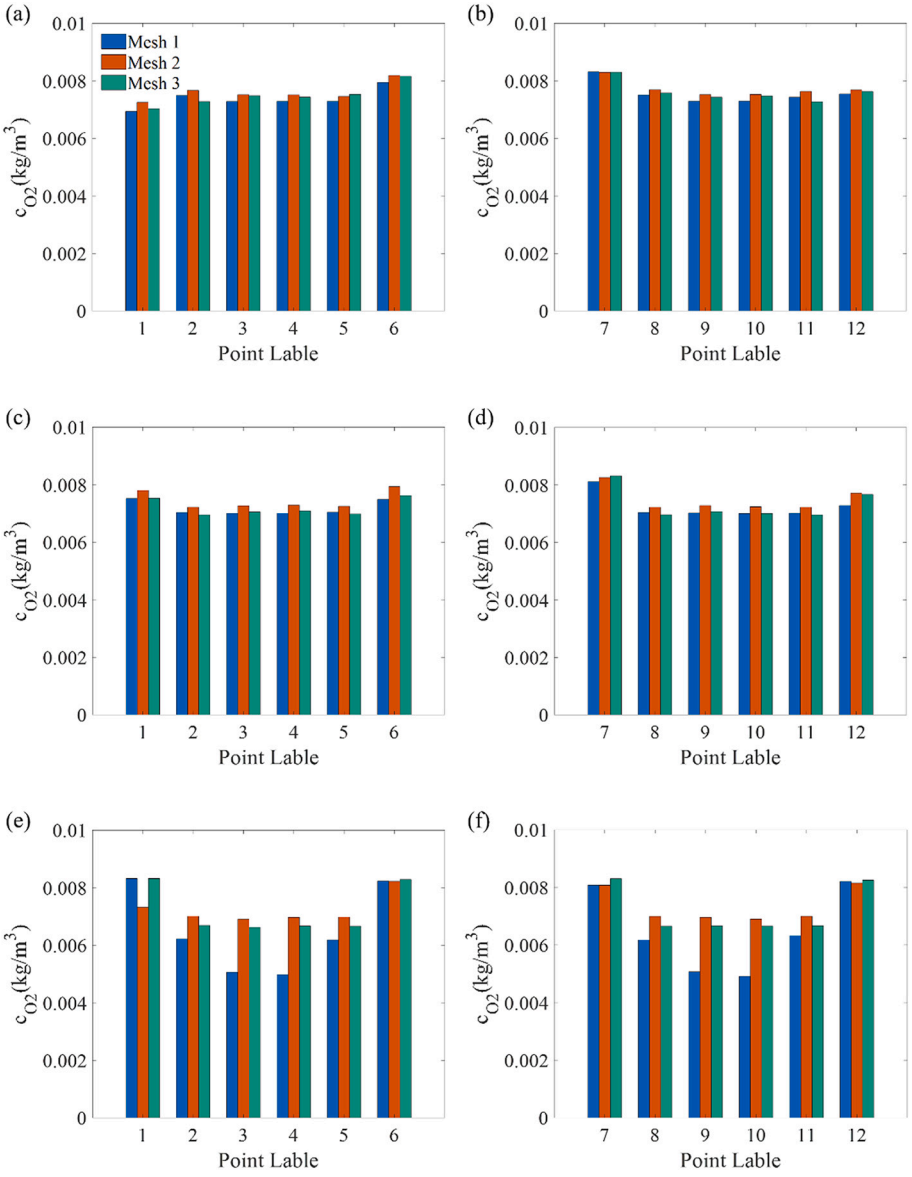

Fig. 4. The DOC values at Points 1– 12 at the steady state at $t = 2000$s at (a), (b) $z = 0.01$m close to the bottom; (c), (d) $z = 0.2$m and (e), (f) $z = 0.39$m close to the water surface.

transport equation of oxygen in the water. The computational domain is divided into a finite number of discrete regions, which is called control volumes or cells. The equations are solved on each cell and the velocity of the flow and DOC in the center of the cell are obtained. The volume of fluid (VOF) method developed by Hirt and Nichols (1981) is used to carry out the multiphase flow simulation and capture the interface between the air and the water. This method relies on the definition of an indicator function, which indicates whether the cell is occupied by one fluid or another, or a mix of both.

The incompressible viscous flows of two immiscible fluids, i.e. air and water, are governed by Navier-Stokes equations. Since Reynolds number (defined as $Re = Ud/\nu$ based on the inlet velocity $U = 2.12$m/s and the inlet diameter of the aquaculture tanks $d = 0.05$m. The kinematic viscosity of the water ($\nu = 1 \times 10^{-6}$m^2/s) of the present study is high ($Re = 106000$), turbulence effects are considered in the present study. VOF method is applied to capture the free surface. The governing equations of the fluids for the mass conservation and momentum conservation are given as

$$\nabla \cdot \mathbf{u} = \mathbf{0} \tag{1}$$

$$\frac{\partial \rho \mathbf{u}}{\partial t} + \nabla \cdot \left(\rho \mathbf{u}\mathbf{u}^{T}\right) = \nabla \cdot \left[(\mu + \mu_{T})\left(\nabla \mathbf{u} + \nabla \mathbf{u}^{T}\right)\right] - \nabla p_{rgh} - (\boldsymbol{g} \cdot \boldsymbol{x})\nabla \rho \tag{2}$$

where $\mathbf{u}$ is the mean velocity vector and 'T' denotes the transpose of the velocity vector. u_1,u_2 (also denoted as u_x and u_y) are the two horizontal velocities and u_3 (also denoted as u_z) is the vertical velocity. ρ is the fluid density with $\rho_{air} = 1.0$kg/m^3 and $\rho_{water} = 1000$kg/m^3; μ is the dynamic molecular viscosity with $\mu_{air} = 1.83 \times 10^{-5}$Ns/m^2 and $\mu_{water} = 1.0 \times 10^{-3}$Ns/m^2; μ_T is the eddy viscosity which accounts for the turbulence effects and is obtained based on the $k - \omega$ turbulence model. p_{rgh} is the pressure in excess of the static pressure defined as $p_{rgh} = p - \rho \boldsymbol{g} \cdot \boldsymbol{x}$; $\boldsymbol{g}$ is the gravitational acceleration; $\boldsymbol{x} = (x_1, x_2, x_3)$ are the Cartesian coordinates. x_1 and x_2 are in the horizontal direction (also denoted as x, y) and x_3 is in the vertical direction (denoted as z).

In order to capture the interphase between the two fluids, an additional equation has to be solved

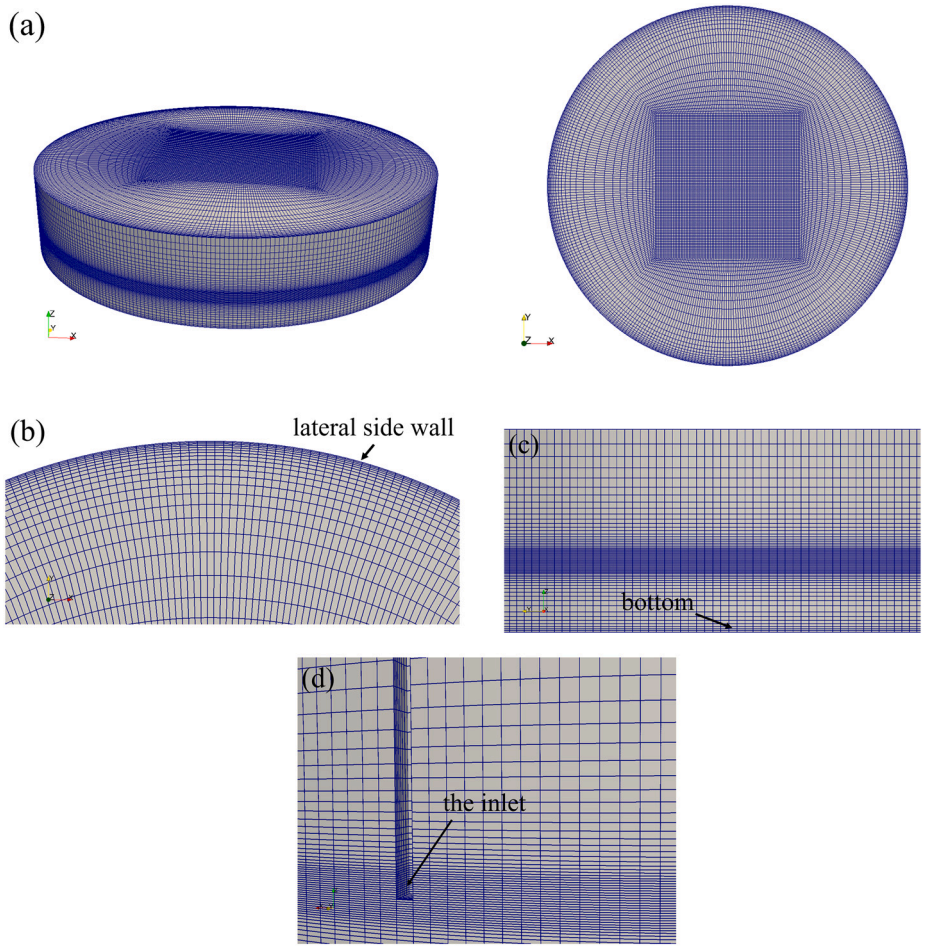

Fig. 5. An example of the meshes (a) full views of the meshes; (b) a zoom-in view around the lateral side wall; (c) a zoom-in view around the water surface and the bottom; (d) a zoom-in view around the inlet.

$$\frac{\partial \alpha}{\partial t} + \nabla \cdot (\mathbf{u}\alpha) = 0 \tag{3}$$

In this equation, α is the volume fraction of water and the volume fraction of air is $1 - \alpha$. The surface tension effects are negligible. The fluid properties such as velocity, density and dynamic viscosity are calculated based on the volume fraction of each fluids as

$$\chi = \alpha \chi_{\text{water}} + (1 - \alpha)\chi_{\text{air}} \tag{4}$$

where χ is a fluid property. An example of a cell in the water-air interface are shown in Fig. 1.

2.2. Oxygen transport

For the DOC in the water, an additional species transport equation for the DOC value c_{O_2} (Marschall et al., 2012) is implemented and solved together with the governing equations Eqs. (1)–(3) of the fluid flow. One of the main challenges in resolving the species transport in two-phase flows is caused by the discontinuity of the diffusion coefficient of the oxygen created by the phase interface. Haroun et al. (2010) overcomes this challenge by introducing an additional discontinuity term in a single species transport equation which is given as

$$\frac{\partial c_{O_2}}{\partial t} + \nabla \cdot (\mathbf{u} c_{O_2}) = \nabla (D c_{O_2}) + \nabla \cdot \left(D \left(\frac{(He - 1) c_{O_2}}{\alpha He + (1 - \alpha)} \right) \nabla \alpha \right) \tag{5}$$

In the equation, the final term in the right hand is the discontinuity term. According to Teuber et al. (2019), the DOC value c_{O_2} is calculated based on its value in the water and in the air as

$$c_{O_2} = \alpha c_{O_2,\text{water}} + (1 - \alpha) c_{O_2,\text{air}} \tag{6}$$

The diffusive coefficient is calculated by $D = D_{\text{phys}} + D_{\text{turb}}$. In this formula, the turbulent diffusivity D_{turb} is calculated by $D_{\text{turb}} = \mu_T/(\rho Sc)$ with the turbulent Schmidt number $Sc = 0.7$ as used in Yin et al. (2018). The physical diffusivity D_{phys} is obtained using a harmonic average value of D_l and D_g which are the diffusion coefficients of the oxygen in the water and the air, respectively as

$$D_{\text{phys}} = \frac{D_l D_g}{\alpha D_l + (1 - \alpha) D_g} \tag{7}$$

He is the nondimensional Henry constant defined as the ratio between the concentration in the water and in the air. Based on Sander (2015), this value is temperature dependent and can be calculated using van't Hoff equation given as

$$He^{\text{cp}}(T) = He^{\text{cp}}(T^{\phi}) exp\left(C \left(\frac{1}{T} - \frac{1}{T^{\phi}} \right) \right) \tag{8}$$

combine with the relationship between the nondimensional He and the dimensional He^{cp}

$$He = He^{\text{cp}}(T) RT \tag{9}$$

In these two equations, C is a temperature coefficient and takes the value of 1700 K according to Sander (2015) and is the standard

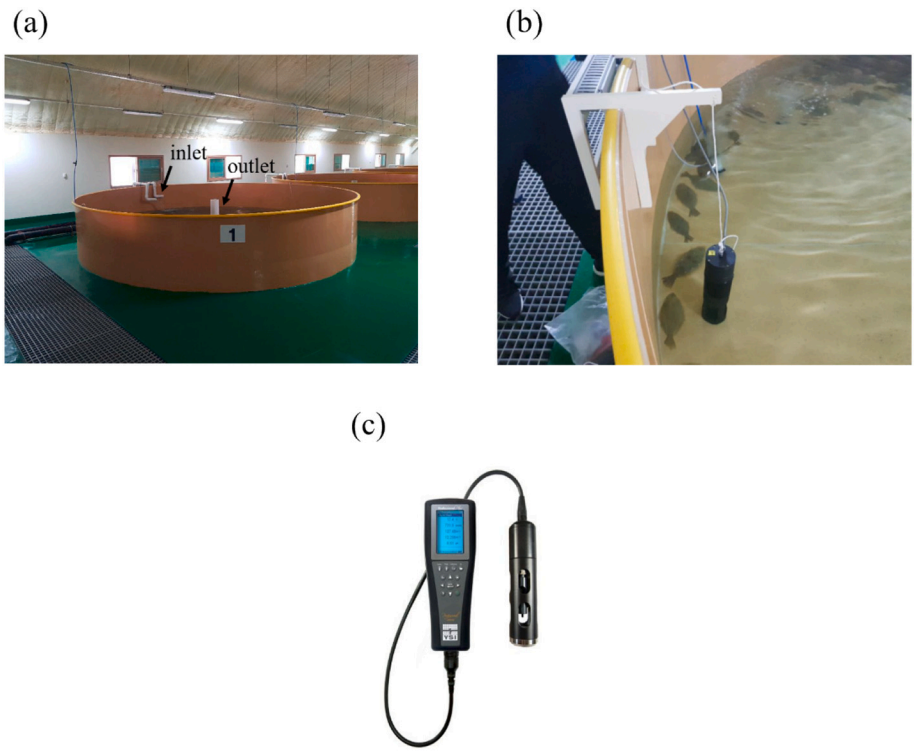

Fig. 6. (a) The actual circular aquaculture tank; (b) The location of the sensor; (c) YSI Professional Plus Multi-parameter Instrument.

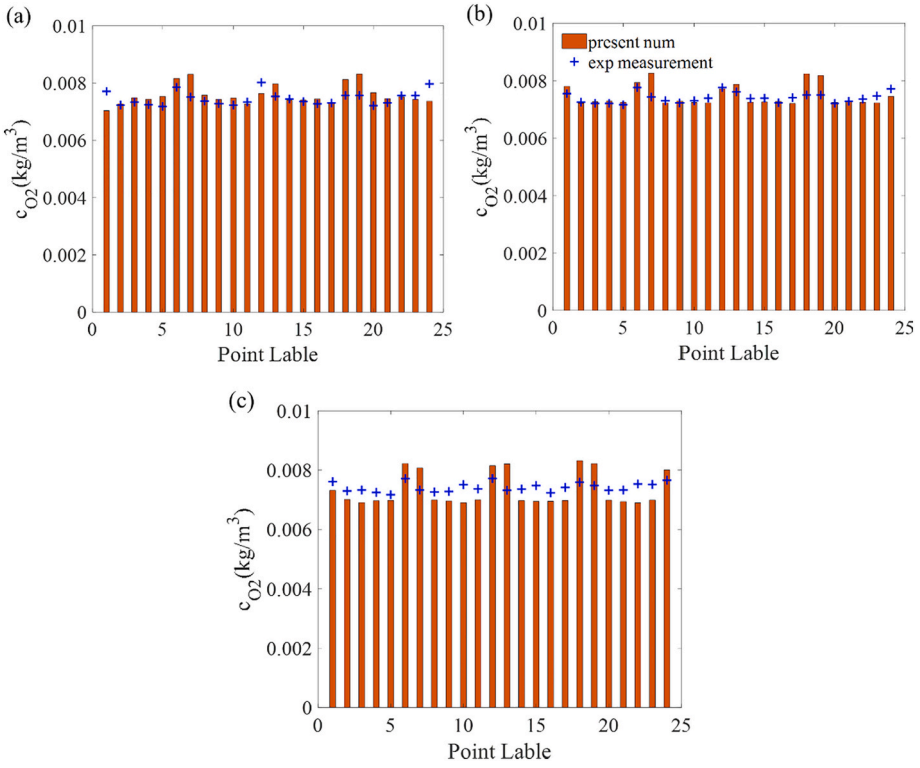

Fig. 7. The DOC values at the detection points obtained by the present numerical simulations at the final steady stage and the experimental measurement and different water levels of (a) $z = 0.01$m close to the bottom; (b) $z = 0.2$m and (c) $z = 0.39$m close to the water surface.

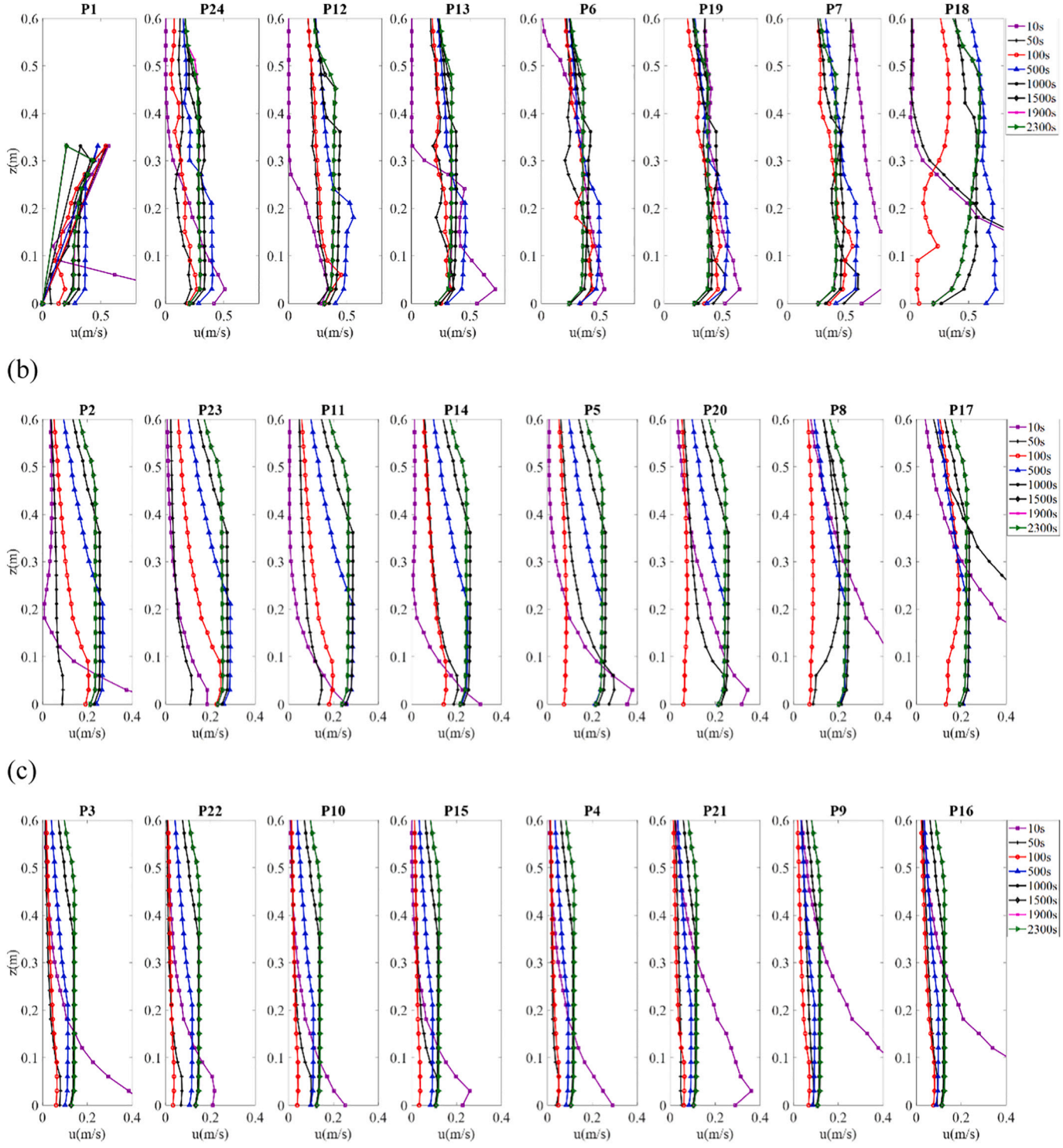

Fig. 8. The profiles of velocity magnitudes on 2D XY planes along the bottom-normal direction at different time instants of t = 10s, 50s, 100s, 500s, 1000s, 1500s, 1900s and 2300s at different detection points on (a) Circle 1; (b) Circle 2; (c) Circle 3.

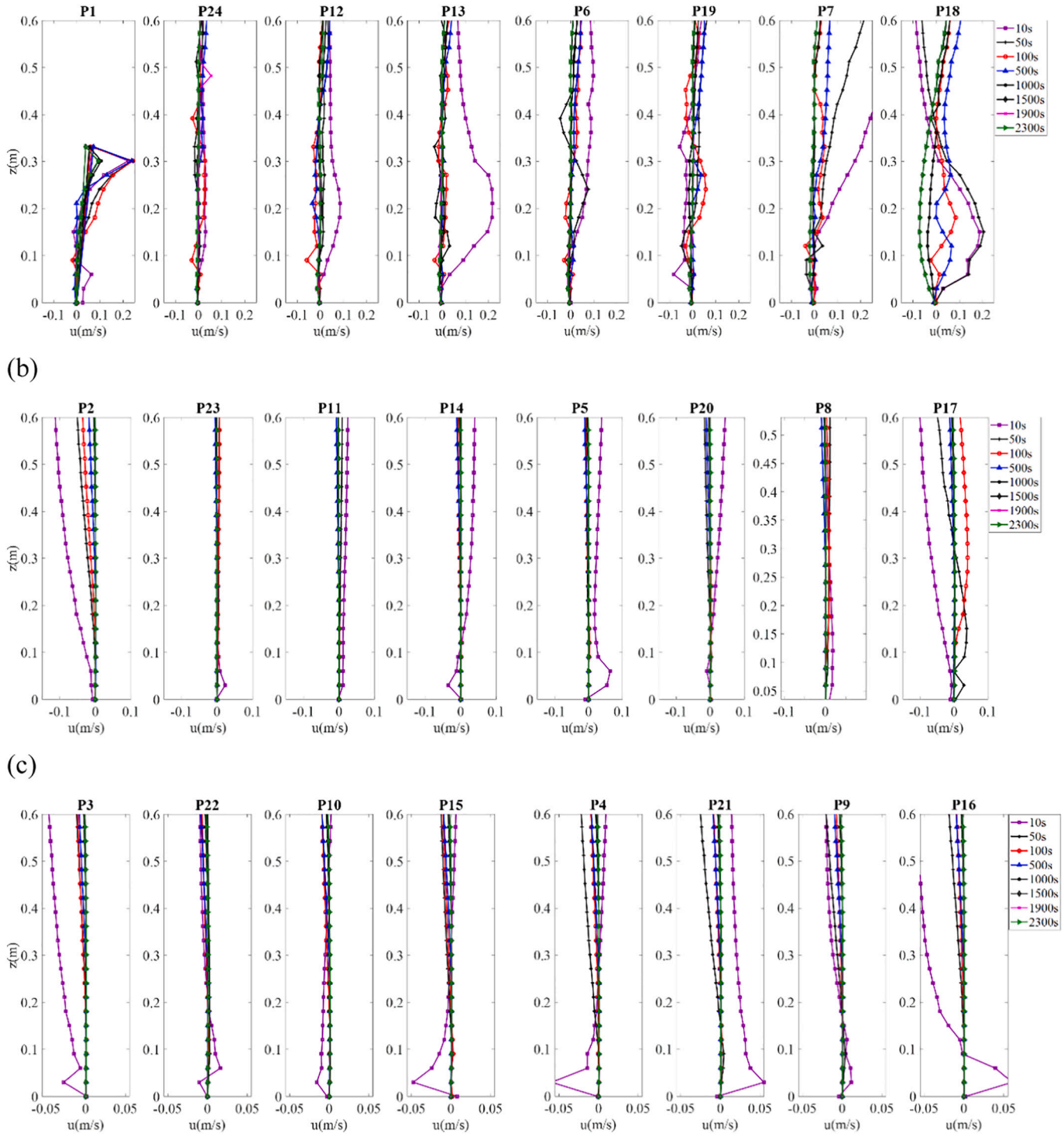

Fig. 9. The profiles of vertical velocities on 2D XY planes along the bottom-normal direction at different time instants of t = 10s, 50s, 100s, 500s, 1000s, 1500s, 1900s and 2300s at different detection points on (a) Circle 1; (b) Circle 2; (c) Circle 3.

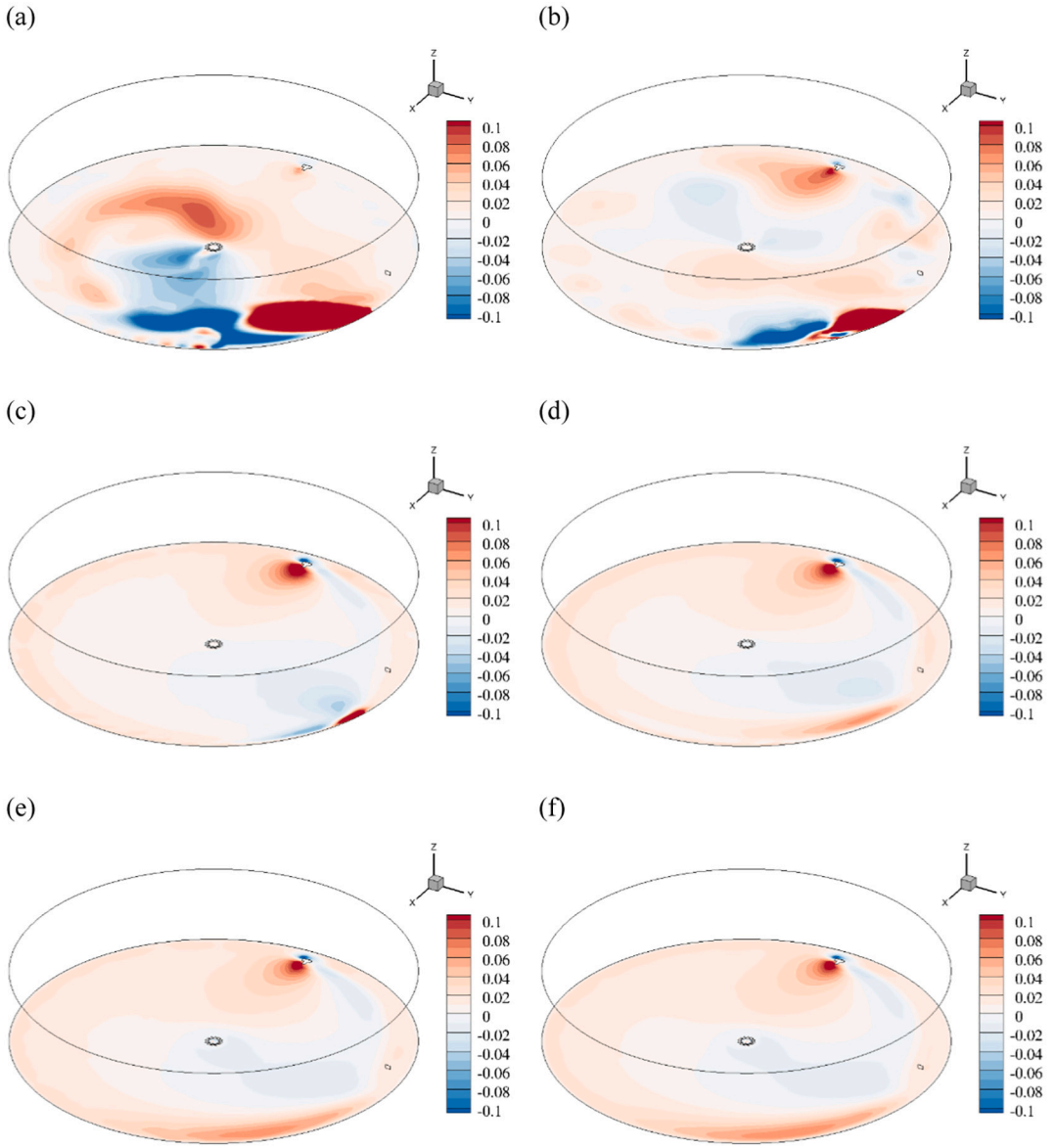

Fig. 10. The radial velocity u_r (m/s) contours at $z = 0.01$m near the bottom at (a) $t = 50s$; (b) $t = 100s$; (c) $t = 500s$; (d) $t = 1000s$; (e) $t = 1500s$; (f) $t = 2300s$.

temperature 298.15 K corresponding to 25°C and R is the universal gas constant. For the diffusive coefficients D_l and D_g, according to Schmitz et al. (2013), the values $D_l = 1.9 \times 10^{-9}\text{m}^2/\text{s}$ and $D_g = 1.98 \times 10^{-5}\text{m}^2/\text{s}$ are used in the present study.

2.3. Computational domains and boundary conditions

In the present study, flows in one land-based aquaculture tank are considered. The flow conditions are set according to the experimental measurement which is stated below. The shape of the land-based aquaculture tank as shown in Fig. 2. (a) is circular with a diameter of $D = 5$m and a height of $H = 1.0$m. The outlet is a circular cylinder with a height of $h = 0.4$m, which is located in the center of the fish tank to keep a fixed water level of 0.4m at the final steady state. The diameter of the outlet is $d = 0.2$m. A sensor is placed with a distance of $h = 0.01$m to the bottom wall and is close to the side wall of the aquaculture tank. The purpose of placing the sensor in the numerical simulations is merely to simulate the experimental set up and the sensor only acts as a cylindrical obstacle in the computational domain. According to the experimental set up, the diameter of the sensor is 0.1 m, which is small compared with the computational domain size. Therefore, the influence of the sensor shape on the DOC distribution in the computational domain can be neglected. One inlet is placed with a distance of $h = 0.4$m to the bottom wall at the side wall. In the experimental set up, an inlet pipe is placed extremely close to the side wall and the direction of the inlet flow is in the azimuthal direction. To simulate the experimental set up in a simplified manner, a rib is placed on the side wall and an inlet with the same area as the inlet face is placed at the lateral side of the rib in the numerical simulations. An inlet flow velocity in the azimuthal direction can be implemented. Since the size the inlet face is small compared with the whole computational domain, the influence of the rib and the inlet face shapes can be neglected. The 3D and 2D views of the aquaculture tank are shown in Fig. 2 (a). In the experimental measurement, pointwise data of DOC value are detected. These detection points are located on three 2D XY planes at three heights (the bottom at $z = 0.01$m, the middle at $z = 0.2$m and the water surface at $z = 0.39$m) within the water. The locations of these 24 points at one 2D XY plane are on three circles (denoted as Circles 1, 2 and 3) with three different radiuses (R, $2R$ and $3R$ with $R = 0.83$m) shown in Fig. 2 (b). Two arrows in Fig. 2 (b) are used to indicate the locations of the inlet and outlet.

At the inlet, a uniform flow with a fixed flow rate is prescribed. An inlet flow mass of $Q = 15$t/h and flow velocities of $(\mathbf{u} \cdot \mathbf{n}) = 2.12$m/s are

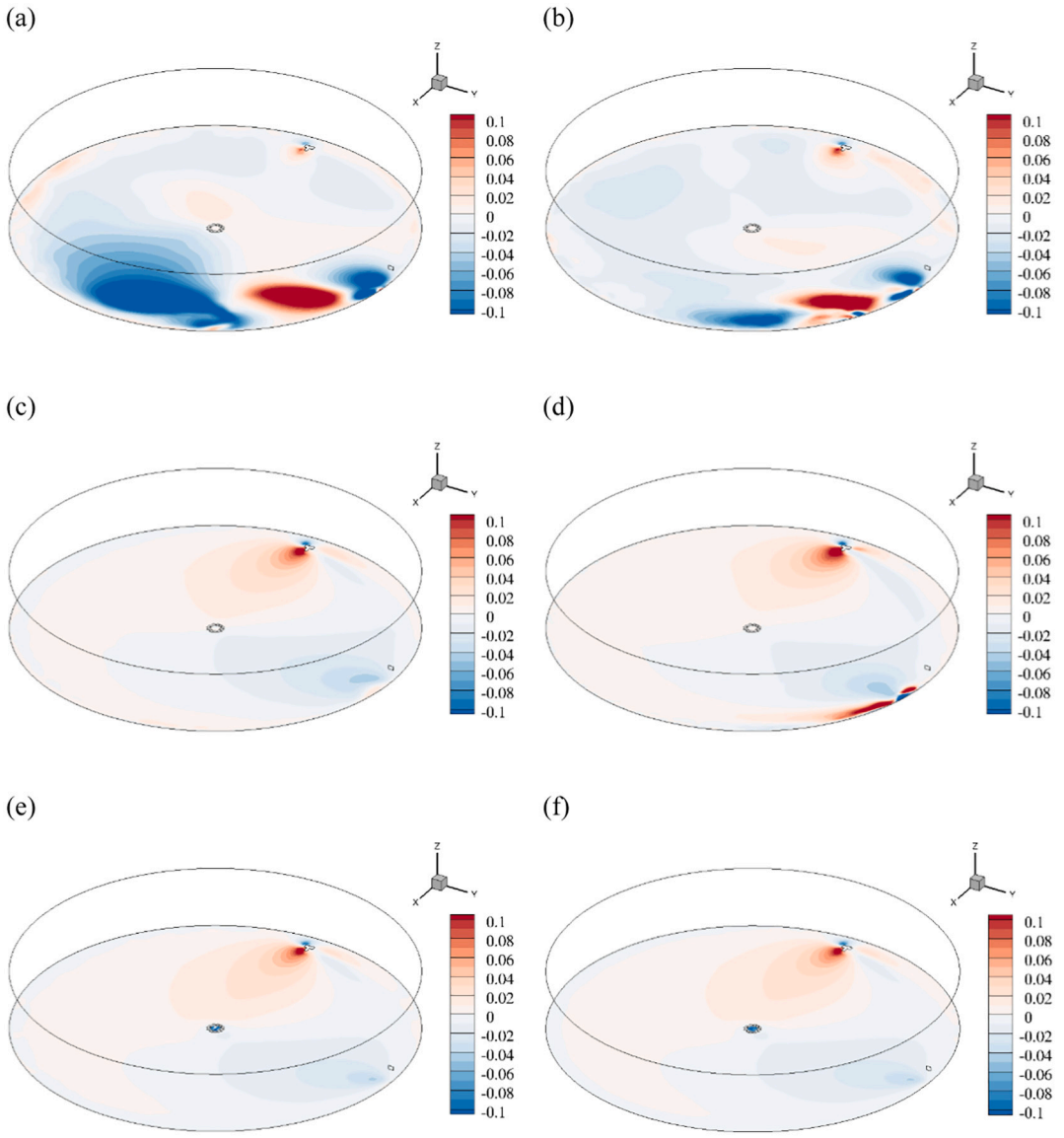

Fig. 11. The radial velocity u_r (m/s) contours at $z = 0.2$m at (a) $t = 50s$; (b) $t = 100s$; (c) $t = 500s$; (d) $t = 1000s$; (e) $t = 1500s$; (f) $t = 2300s$.

used (**n** is the normal unit vector of the inlet face). The pressure is prescribed as zero gradient at the inlet. A fixed DOC value of $c_{O_2} = 0.00826\text{kg/m}^3$ is set at the inlet. At the outlet, the flow velocities are set as zero normal gradient and the pressure is set to be 0. Zero normal gradient is used for the DOC value. On the surface of the horizontal walls of the fish tanks, no-slip boundary condition for the flow velocities is used, i.e. $\mathbf{u} = \mathbf{0}$. The pressure and the DOC value are set as zero normal gradient.

2.4. Convergence studies and validation studies

In the present study, structural meshes are used and the meshes are refined near the inlet face, the bottom and lateral side wall. It also worth mentioning that, due to the small size of the inlet and outlet compared with the size of the aquaculture tank, in the preprocess of the simulations, the inlet and outlet faces are created by removing prescribed faces of some computational grids using utilities of topoSet and createPatch implemented in OpenFOAM. Grid and time-step convergence studies are performed. First, the values of the DOC obtained by using different grid numbers of Mesh 1 (679,296 cells), Mesh 2 (940,531 cells) and Mesh 3 (1,458,955 cells) with a fixed time-step of $\Delta t = 0.001$s are used to evaluate the grid resolutions. For the three heights, the time histories of the DOC at the measurement Points 1–6 of different grid numbers are shown in Fig. 3. It can be seen that when increasing the grid numbers from 679,296 to 1,458,955, the time histories are getting closer to each other. The DOC values at different detection points become steady at $t >$ 1500s. The DOC values at Points 1–12 at $t = 2000$s of the steady state using Meshes 1–3 are shown in Fig. 4. It is shown that at the bottom and the middle height of $z = 0.2$m, the differences of the DOC value for the three meshes are small while at the water surface, the differences between Mesh 1 and Mesh 2 are large. However, for Meshes 2 and 3, the differences are becoming smaller. Therefore, it can be concluded that

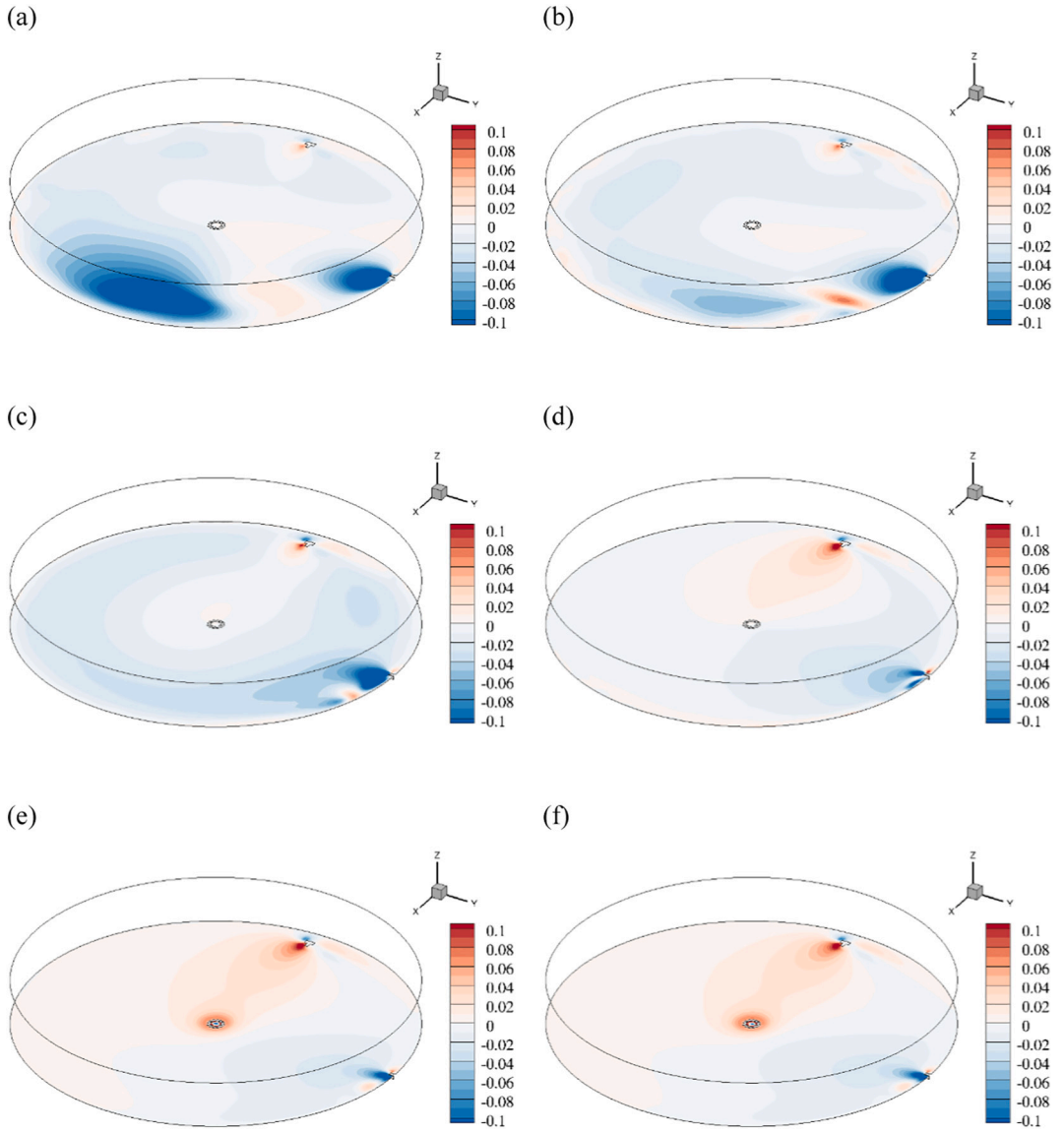

Fig. 12. The radial velocity u_r (m/s) contours at $z = 0.39$m close to the water surface (a) $t = 50s$; (b) $t = 100s$; (c) $t = 500s$; (d) $t = 1000s$; (e) $t = 1500s$; (f) $t = 2300s$.

the grid resolution of Mesh 2 can be regarded as sufficient to provide convergent results based on the predicted DOC value. An overview of the grid of Mesh 2 and the regions of refinement are shown in Fig. 5. Furthermore, the time-step resolution study is carried out by decreasing the time-step to $\Delta t = 0.0005$s using Mesh 2 and the differences of the DOC value from those using $\Delta t = 0.001$s are within 5%. As a result, the time-step $\Delta t = 0.001$s is sufficient to provide convergent prediction of the DOC value.

Comparisons of the DOC values at these points between the present numerical simulations and the experimental measurement are shown in Fig. 7. The experimental measurement was conducted by Jeju Ocean and Fisheries Research Institute of Korea. The actual circular aquaculture tank is shown in Figs. 6 (a) and (b). The locations of the inlet, outlet and the sensor are indicated in the figures. All the measurement data was obtained at the steady state when the water level in the aquaculture tank is kept at $z = 0.4$m. A YSI Professional Plus Multi-parameter Instrument shown in Fig. 6 (c) was used to carry out pointwise measurement of the DOC. It can be seen that at the bottom and the middle part $z = 0.2$m of the circular tank, the numerical predicted DOC values are close to the experimental data while around the water surface of $z = 0.4$m, due to the sensitivity in capturing interface between the two phases, there are differences between the numerical simulation results and the experimental measurement and the maximum relative differences is less than 10%. In general, the present numerical model can provide trustful prediction of DOC values within the water.

3. Results and discussion

Results are presented in terms of the flow velocity and the DOC in the water. All the discussion is based on the results obtained by using Mesh 2 with a simulation time-step of $\Delta t = 0.001$s.

3.1. Velocity distributions

The profiles of velocity magnitudes on 2D XY planes calculated by $u = \sqrt{u_x^2 + u_y^2}$ along the bottom-normal direction at different time instants in the range of $t = 10$s~2300s are shown in Fig. 8. At the late time instants of $t \geq 1500$s when the overall water flow tends to be steady, the velocity magnitudes at each detection point along the three circles in the aquaculture tank tend to be similar for different points and also uniform along the bottom-normal direction up to the water surface. The velocity magnitudes along the detection circles from Circle 1 to

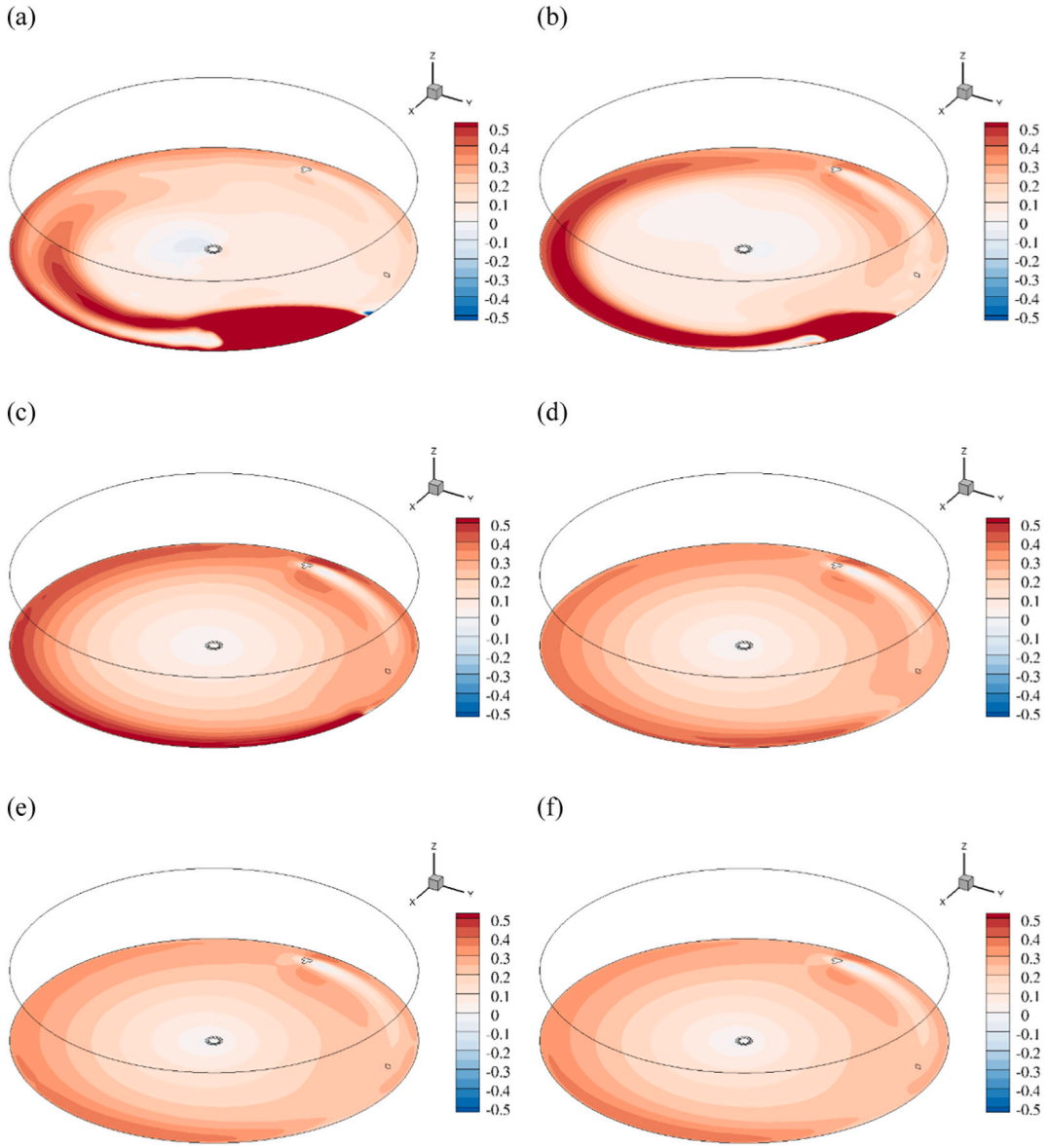

Fig. 13. The azimuthal velocity u_θ (m/s) contours at $z = 0.01$m near the bottom at (a) $t = 50s$; (b) $t = 100s$; (c) $t = 500s$; (d) $t = 1000s$; (e) $t = 1500s$; (f) $t = 2300s$.

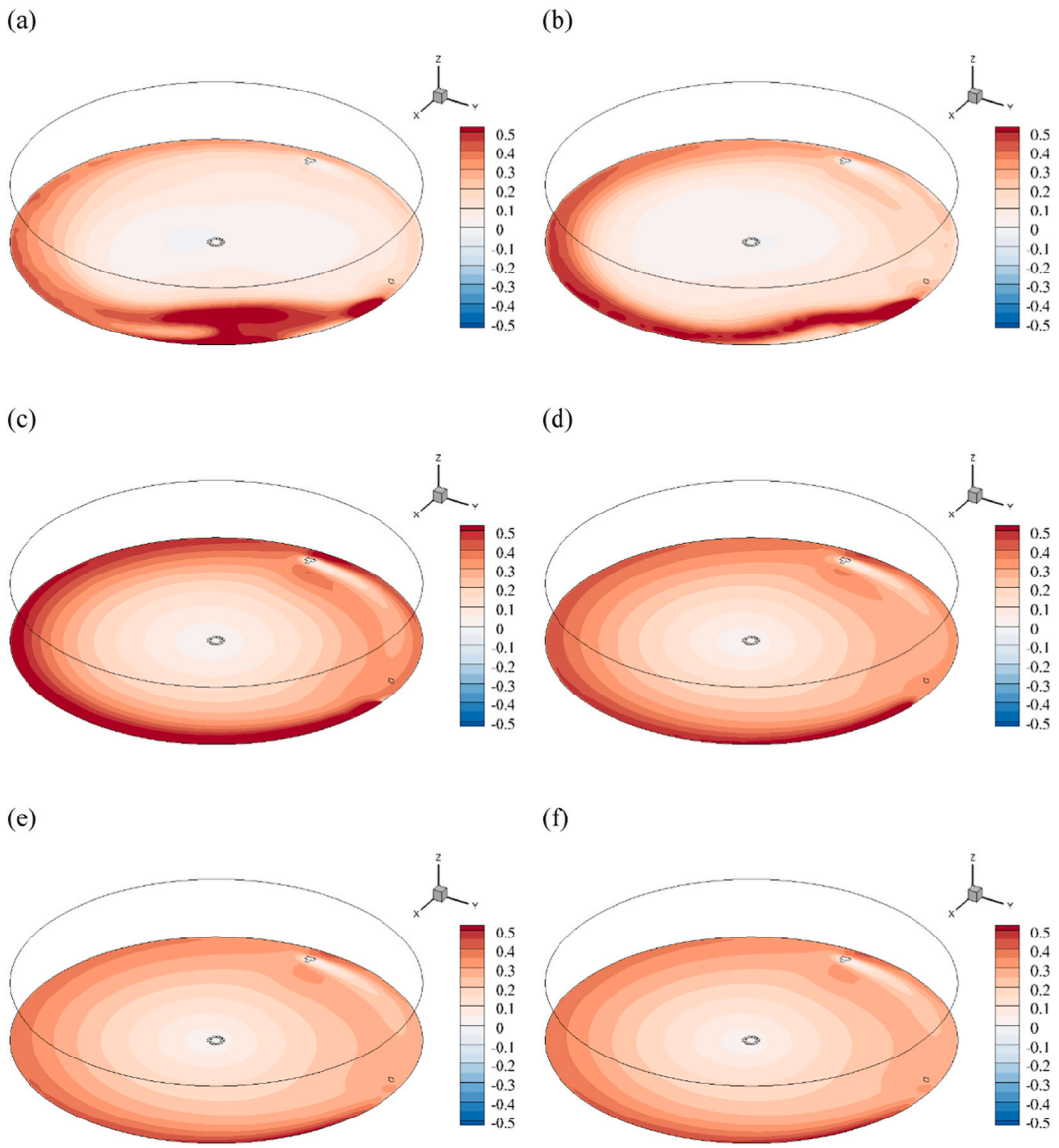

Fig. 14. The azimuthal velocity u_θ (m/s) contours at $z = 0.2$m at (a) $t = 50s$; (b) $t = 100s$; (c) $t = 500s$; (d) $t = 1000s$; (e) $t = 1500s$; (f) $t = 2300s$.

Circle 3 are 0.3–0.4 m/s, 0.2–0.25 m/s and 0.1–0.15 m/s, respectively. In additions, it should be noted that the velocity is a phase averaged value between the air and the water as obtained by using Eq. (4). Therefore, at early time instants of $t = 10$s, 50s when the water level has not reached to the outlet, the velocity of the air is larger than 0, and at all detection points, the velocity magnitudes are large as the water flows past these points. Because the inlet is placed close to the side wall of the aquaculture tank and the inlet flow velocity is along the azimuthal direction, the velocity magnitudes at the detection points on Circle 1 near the side wall are large at the early time instants of $t \leq 50$s. The velocity magnitudes at these detection points are gradually reduced with the increasing water level due to the water flowing into the center part of the aquaculture tank. At the detection points on Circle 3 close to the center of the aquaculture tank, the velocity magnitudes increase with the increasing water level at $t \geq 100$s due to the continuous water flowing from the outer part of the aquaculture tank through Circle 3.

The vertical velocities along the bottom-normal direction at different time instants in the range of $t = 10$s~2300s are shown in Fig. 9. At the early time instants of $t = 10$s, the downwards flow of the water causes large negative vertical velocities close to the water surface and reach to 0 down to the tank bottom. At the final steady state and at all the detection points, the vertical velocities tend to the 0 along the bottom-normal direction, which indicates weak flow in the vertical direction.

The contours of the flow velocities on the 2D XY plane at three heights of $z = 0.01$m, 0.2m and 0.39m are shown in Figs. 10-15. For the radial velocity u_r (obtained by $u_r = -(u_x \cos\theta + u_y \sin\theta)$ where $cos\theta = y/\sqrt{x^2+y^2}$ and the positive u_r direction is towards the center of the tank), it can be seen that at the early time instants of $t = 50$s and 100s when the water level is low, the radial velocity is large close to the inlet on the 2D XY plane at $z = 0.01$m near the tank bottom, indicating strong water flow both towards and outwards the center of the tank. The water flow at these time step seems to be chaotic. At the late time instants of $t \geq 1000s$, the water flow tends to be steady, and at the outer part of the tank, the radial velocity is generally positive indicating there is still strong water flow towards the center of the tank at the steady state. At the two higher locations of $z = 0.01$m and 0.2m, the radial velocity is smaller compared with that at $z = 0.39$m, which means that the flow in the radial direction is weak.

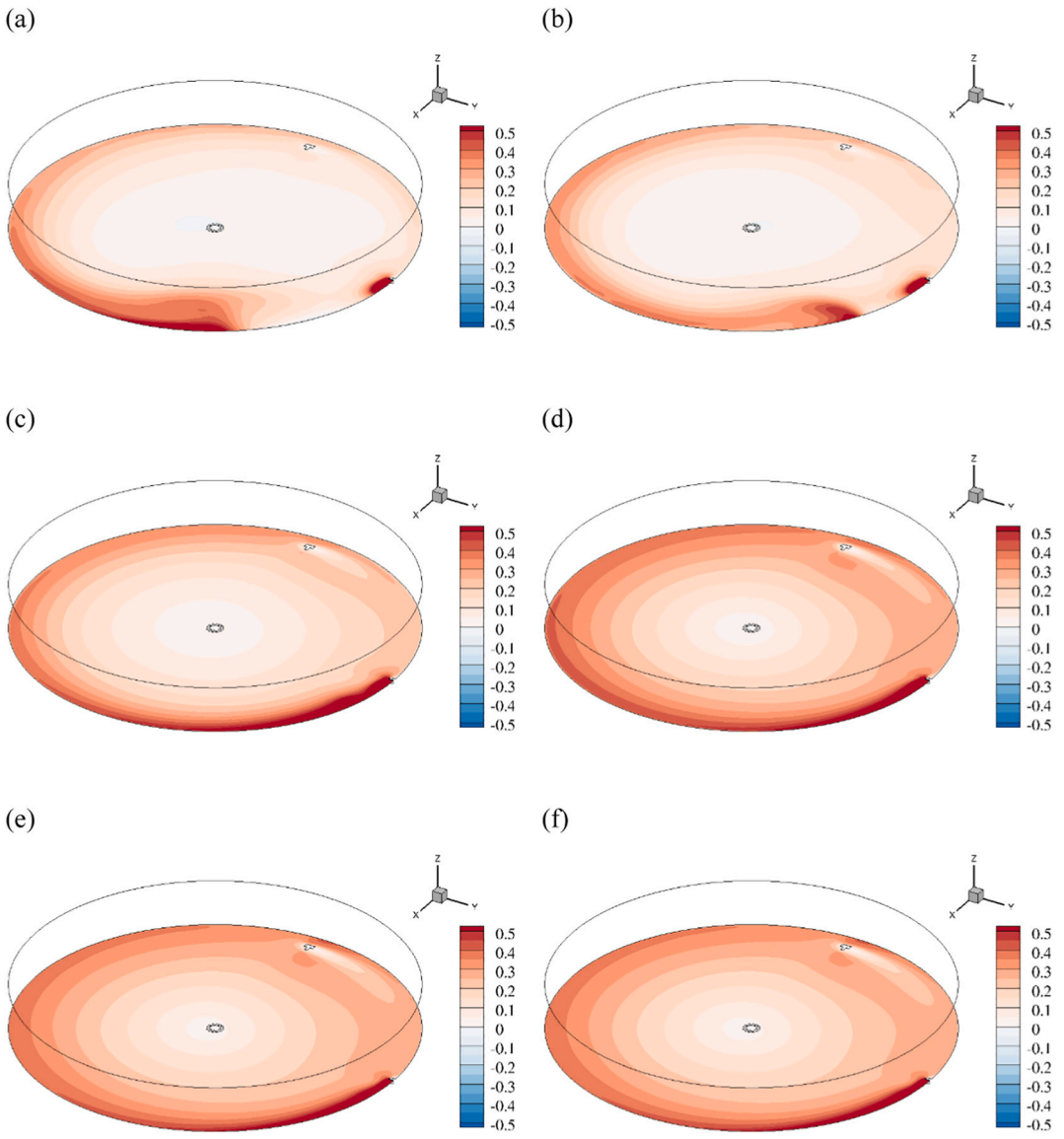

Fig. 15. The azimuthal velocity u_θ (m/s) contours at $z = 0.39$m close to the water surface at (a) $t = 50s$; (b) $t = 100s$; (c) $t = 500s$; (d) $t = 1000s$; (e) $t = 1500s$; (f) $t = 2300s$.

For the azimuthal velocity u_θ (obtained by $u_\theta = (u_x \sin\theta - u_y \cos\theta)$ with the positive values denoting the clockwise azimuthal direction and the negative values denoting the counterclockwise azimuthal direction), the value is large indicating that the water flow is mainly in the azimuthal direction. The area of the large absolute value of clockwise azimuthal velocity is expanded towards the center of the tank. At the late time instants of $t \geq 1000$s, the values of u_θ distribution become homogenous along the radial direction. Furthermore, the values of u_θ tend to be similar at the three heights.

3.2. DOC distributions

The time evolution of the DOC isosurface ($c_{O2} = 0.005$mg/L) colored by the magnitude of the velocity (m/s) are shown in Fig. 16. Within the time of $t \leq 400$s, as the flow goes from the inlet along the side wall, high DOC is distributed near the side wall. Due to the diffusion of the oxygen and the effects of the turbulent diffusion in the water, the DOC is gradually distributed in the radial direction to the center of the fish tank. The speed of the DOC value diffusion towards the center of the tank is uniform along the azimuthal direction. At $t = 1500$s when the flow reaches a steady state, the DOC distribution tends to be homogenous within the tank.

The contour of the DOC value on the 2D plane in YZ view are shown in Fig. 17 at different time instants of $t = 50$s~2300s. At the early time instants of $t = 50$s, due to the presence of the bottom wall, oxygen gathers around the bottom wall and diffuses faster to the center along the bottom and near the water surface than at the middle region. At $t \geq 1200s$ after the water level reaches the outlet, there is water flowing out through the outlet and the oxygen is also transported out of the outlet from the middle of the tank. At the final stage, the tank is overall full of the oxygen and the DOC value is slightly lower around corner of the outlet pipe compared with other regions in the tank. As seen in Fig. 8, the flow velocities are much lower in the center part of the tank compared with the outer part. Therefore, the transport of oxygen in the center part of the tank is mainly determined by the oxygen diffusion in the water and the transport speed is much smaller than that caused by flow motions, which may lead to the lower level of DOC compared with the outer part of the tank.

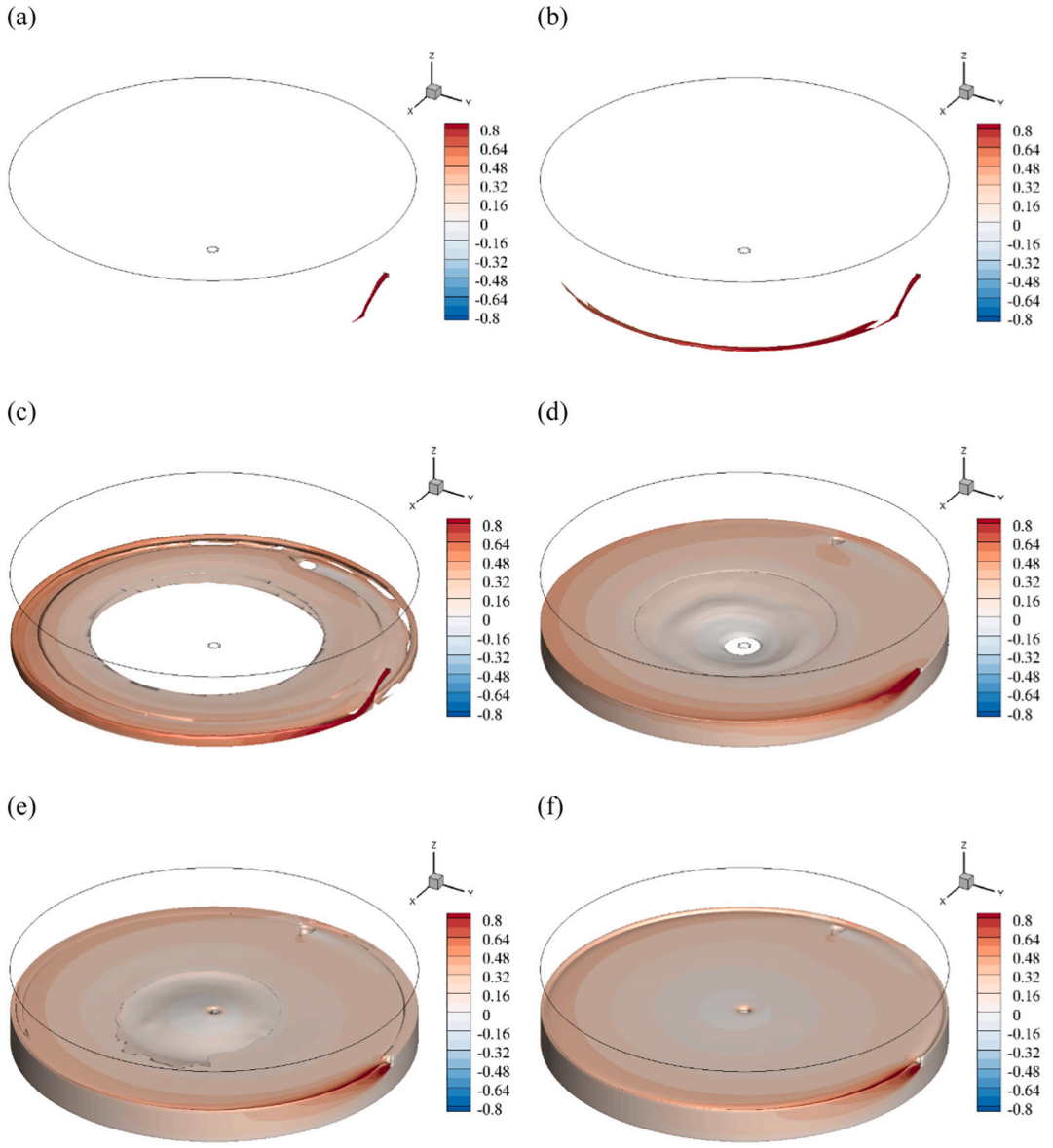

Fig. 16. The DOC isosurface ($c_{O2} = 0.005 kg/m^3$) colored by the magnitude of the velocity (m/s) at (a) $t = 50s$; (b) $t = 300s$; (c) $t = 500s$; (d) $t = 1000s$; (e) $t = 1500s$; (f) $t = 2300s$.

4. Conclusion

The dissolved oxygen concentration (DOC) distribution in a land-based aquaculture tank is important for the survival of fish. In the present study, a three-dimensional numerical simulation is used to investigate the evolution of DOC in the aquaculture. The water-air interface is captured by the volume of fluid (VOF) method. An additional convection-diffusion equation for the oxygen transport is solved taking consideration of the different diffusion coefficients of the oxygen across the air-water interface. The numerical model is validated against the experimental measurements of DOC values at different detection points at the final steady state. The main conclusions can be outlined as following:

1. At the time instants of $t \geq 1500s$ when the overall water flow in the aquaculture tank is steady and the velocity magnitudes at each detection point along the three circles on 2D XY planes are similar and uniform along the bottom-normal direction up to the water surface. The vertical velocities along the bottom-normal direction at the final steady state are close to the 0 along the bottom-normal direction, which means that the flow in the vertical direction is weak in the aquaculture tank.
2. At the final steady stage and the outer part of the tank, the water flow goes towards the center of the tank and the radial velocity is generally positive. At the height close to the water surface and the flow in the radial direction is weak. The water flow is mainly in the azimuthal direction. The area of the large absolute value of azimuthal velocity is expanded towards the center of the tank and its value becomes homogenous along the radial direction.
3. DOC is gradually distributed in the radial direction to the center of the aquaculture tank by the effects of the turbulent diffusion in the water. The oxygen diffuses faster to the center of the aquaculture tank along the bottom and near the water surface than at the middle region. When the flow reaches a steady state, the DOC distribution is homogenous within the tank while the DOC value is slightly lower

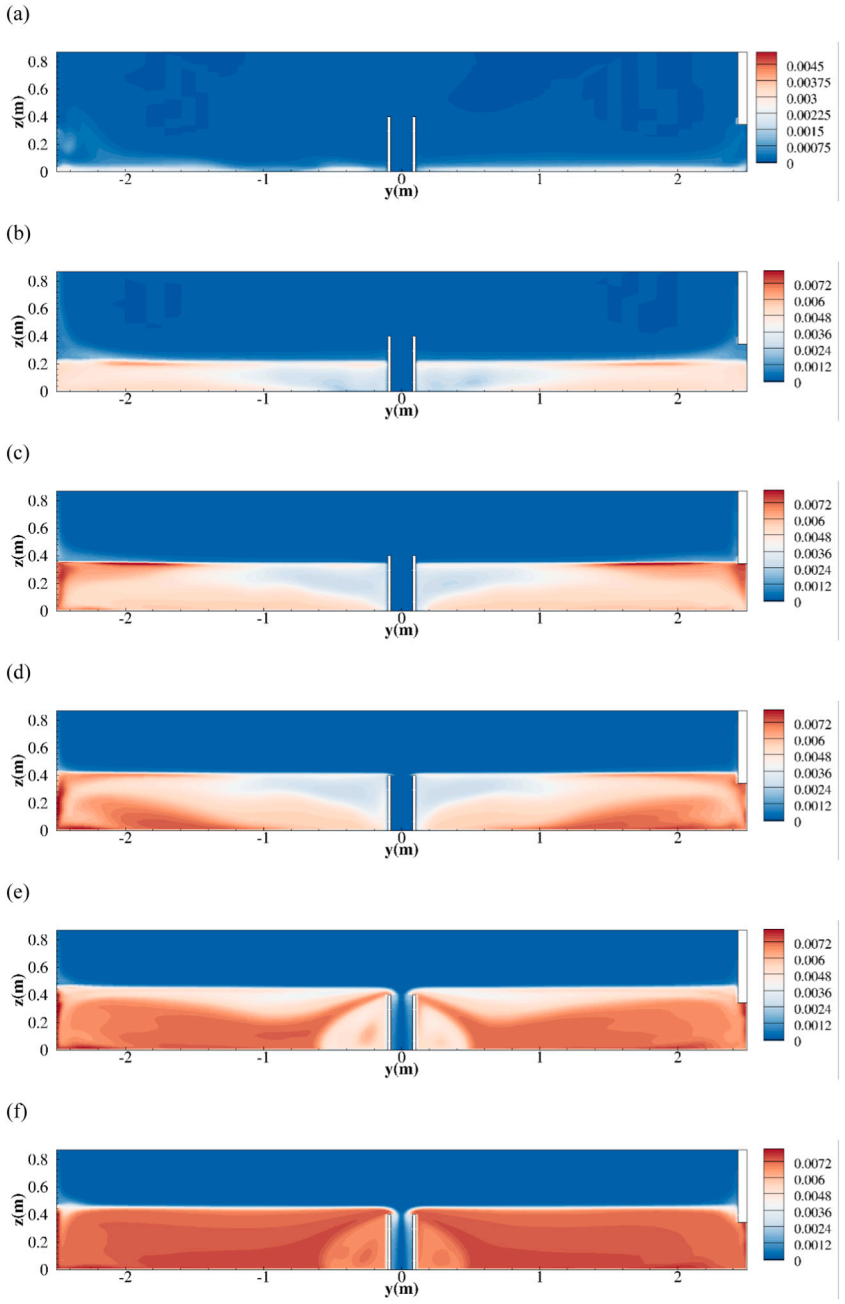

Fig. 17. The DOC contours in the YZ plane at different time instants of (a) $t = 50s$; (b) $t = 500s$; (c) $t = 1000s$; (d) $t = 1200s$; (e) $t = 1500s$; (f) $t = 2300s$.

around corner of the outlet pipe compared with other regions in the tank.

The CFD simulation model developed in the present study can be useful for researchers in aquaculture engineering to solve the complex flow problems and avoid high cost of experimental set up for actual measurement of DOC in land-based aquaculture tanks with different configurations. Furthermore, the CFD model might also benefit the optimal design of oxygen aeration systems for aquaculture.

Declaration of Competing Interest

We declare that all authors have no conflicts of interest to this work.

Acknowledgments

This research was a part of the project titled “Smart Aquaculture Research Center”, funded by the Ministry of Oceans and Fisheries, Korea.

References

Böttger, S.A., Devin, M.G., Walker, C.W., 2006. Suspension of annual gametogenesis in north American green sea urchins (Strongylocentrotus droebachiensis) experiencing invariant photoperiod—applications for land-based aquaculture. Aquaculture 261 (4), 1422–1431.

Cheng, X., Chen, X., Chen, Y., 2009. Numerical simulation of dissolved oxygen concentration in the downstream of three gorges dam. In: World Environmental and Water Resources Congress 2009: Great Rivers, pp. 1–11.

Fayolle, Y., Cockx, A., Gillot, S., Roustan, M., Héduit, A., 2007. Oxygen transfer prediction in aeration tanks using CFD. Chem. Eng. Sci. 62 (24), 7163–7171.

Guo, X., Zhou, X., Chen, Q., Liu, J., 2013. Flow field and dissolved oxygen distributions in the outer channel of the orbal oxidation ditch by monitor and CFD simulation. J. Environ. Sci. 25 (4), 645–651.
Haroun, Y., Legendre, D., Raynal, L., 2010. Volume of fluid method for interfacial reactive mass transfer: application to stable liquid film. Chem. Eng. Sci. 65 (10), 2896–2909.
Hirt, C.W., Nichols, B.D., 1981. Volume of fluid (VOF) method for the dynamics of free boundaries. J. Comput. Phys. 39 (1), 201–225.
Kim, T., Yoon, H.S., Shin, S., Oh, M.H., Kwon, I., Lee, J., Choi, S.D., Jeong, K.S., 2015. Physical and biological evaluation of co-culture cage systems for grow-out of juvenile abalone, *Haliotis discus hannai*, with juvenile sea cucumber, *Apostichopus japonicus* (Selenka), with CFD analysis and indoor seawater tanks. Aquaculture 447, 86–101.
Liu, S., Ong, M.C., Obhrai, C., Seng, S., 2017. Numerical simulations of regular and irregular wave forces on a horizontal semi-submerged cylinder. In: ASME 2017 36th International Conference on Ocean, Offshore and Arctic Engineering. American Society of Mechanical Engineers Digital Collection.
Marschall, H., Hinterberger, K., Schüler, C., Habla, F., Hinrichsen, O., 2012. Numerical simulation of species transfer across fluid interfaces in free-surface flows using OpenFOAM. Chem. Eng. Sci. 78, 111–127.
Matko, T., Chew, J., Wenk, J., Chang, J., Hofman, J., 2020. Computational fluid dynamics simulation of two-phase flow and dissolved oxygen in a wastewater treatment oxidation ditch. Process Saf. Environ. Prot. 145, 340–353.
Sander, R., 2015. Compilation of Henry's law constants (version 4.0) for water as solvent. Atmos. Chem. Phys 15 (8), 4399–4981.
Schmitz, D., Anlauf, R., Rehrmann, P., 2013. Effect of air content on the oxygen diffusion coefficient of growing media. Am. J. Plant Sci. 4 (5), 955–963.
Teuber, K., Broecker, T., Bentzen, T.R., Stephan, D., Nützmann, G., Hinkelmann, R., 2019. Using computational fluid dynamics to describe H_2S mass transfer across the water-air interface in sewers. Water Sci. Technol. 79 (10), 1934–1946.
Xia, M., Craig, P.M., Wallen, C.M., Stoddard, A., Mandrup-Poulsen, J., Peng, M., Schaefffer, M., Liu, Z., 2011. Numerical simulation of salinity and dissolved oxygen at Perdido Bay and adjacent coastal ocean. J. Coast. Res. 27 (1), 73–86.
Yin, Z., Zhang, L., Cao, X., Wang, L., Cheng, D., 2011. Dissolved oxygen convection and diffusion numerical simulation of stokes wave. In: 2011 International Symposium on Water Resource and Environmental Protection, Vol. 3. IEEE, pp. 1995–1998.
Yin, Z.G., Cao, X.W., Cheng, D.S., Wang, L., 2012. Dissolved oxygen convection and diffusion numerical simulation of water and air mixture flow in circular pipe. In: Advanced Materials Research, Vol. 383. Trans tech publications ltd, pp. 6651–6656.
Yin, Z., Feng, Y., Wang, Y., Gao, C., Ma, N., 2018. 3-D numerical investigation on oxygen transfer in a horizontal venturi flow with two holes. Water 10 (2), 1–13.